Numerical Modeling of the Plasmakristall-4 Experiment on the ISS

Katrina Vermillion[1], Abbie Terrell[1], Emerson Gehr[1], Evdokiya Kostadinova[1,2], Peter Hartmann[1,3], Lorin Matthews[1], and Truell Hyde[1]

[1]*Center for Astrophysics, Space Physics, and Engineering Research (CASPER) at Baylor University, Waco, TX, 76706, USA*

[2]*Physics Department, Auburn University, Auburn, AL, 36849, USA*

[3]*Institute for Solid State Physics and Optics, Wigner Research Centre for Physics, P.O. Box 49, H-1525 Budapest, Hungary*

The microgravity environment of the Plasmakristall-4 experiment on the International Space Station provides a laboratory for exploring plasma-mediated interactions between charged dust grains in fully three-dimensional space. Away from the strong influence of Earth's gravity, the dust grains can levitate in the bulk of the plasma, where they have been observed to form extended filamentary structures along the discharge tube axis and exhibit dust particle lane formation, among other interesting behavior. These formations are expected to provide insight into the mechanisms responsible for the complex interactions between charged dust grains and plasma, serving as an analogue for other self-organizing systems. Here we present the results from numerical modeling performed using N-body molecular dynamics simulations of the ion flow past isolated microstructures within the dust cloud (single dust chains) and the dust cloud macrostructure. Although dust grains are known to respond on the millisecond timescale, analysis reveals that periodic variations of plasma conditions on the microsecond timescale significantly affect dust structure formation. In addition to the expected formation of lanes in the dust cloud macrostructure, dust grains in a large cloud were observed to organize into ordered positions on the surface of nested cylinders.

I. Nomenclature

ε_0	=	vacuum permittivity, [C/(V·m)]
k_B	=	Boltzmann constant, [J/K]
m_i, m_d	=	mass of an ion, mass of a dust grain, [kg]
r, z	=	radial and axial spatial dimensions, [m]
Q_d	=	dust grain charge, [C]
$q_i(q_j)$	=	charge of ion i (j), [C]
λ_{De}	=	electron Debye length, [m]
λ_{Di}	=	ion Debye length, [m]
P_g	=	neutral gas pressure, [Pa]
T_g	=	neutral gas temperature, [K]
a	=	dust grain radius, [m]
Δt_d	=	dust timestep, [s]
Δt_i	=	ion timestep, [s]

II. Introduction

Complex (dusty) plasmas are composed of neutral gas atoms, ions, electrons, and microparticles, commonly referred to as "dust." The dust grains in such an environment typically range in size from nanometers to millimeters and may arise from chemical reactions within the plasma, reactions between the plasma and confining surfaces, or may be introduced from an outside source [1]–[3]. Dust immersed in a plasma environment quickly acquires charge by collecting ions and electrons, and these highly charged dust grains interact in interesting ways with charged plasma particles, electric and magnetic fields, and other charged dust grains [4]–[6]. The acceleration of charged dust grains by an electric field is commonly used to manipulate the dust grains by levitating them against the force of gravity in ground-based experiments. In microgravity experiments, electric fields can be used to transport dust grains through the plasma bulk, or trap the dust grains by applying an electric field that reverses directions at a frequency higher than the dust plasma frequency (through a procedure called "polarity switching").

Complex plasmas have been a useful analogue for studying microscopic phenomena such as crystallization and melting phase transitions, self-organization, and growth of crystalline structures [7]–[12]. The advantages of using dusty plasmas arise from the relative ease of experimentally observing the motions of macroscopic dust grains and the wide range of parameters available, including the neutral gas type, pressure, temperature, plasma density, dust number density, dust material, and dust grain size.

In ground-based complex plasma experiments, dust grains levitate in the sheath of the plasma where strong electric fields are required to balance the gravitational force acting on the dust grains, and, as a result, the dust grains typically organize into quasi-2D structures. Unfortunately, the large influence of the electric and gravitational forces in these experiments limits investigators' ability to probe the smaller-magnitude forces involved in the interactions between the flowing ions and dust grains. In contrast, a microgravity environment like the one on the International Space Station (ISS) allows dust grains to levitate in the plasma bulk where dust-dust and ion-dust interactions are the dominant forces and three-dimensional phenomena including dust particle lane formation, transitions between laminar and turbulent flows, dust acoustic instabilities, and dust waves can be visualized.

The Plasmakristall-4 (PK-4) is a microgravity complex plasma laboratory installed in the Columbus module of the ISS. The PK-4 is capable of generating a direct current (dc) or radio frequency (rf) plasma discharge using argon or neon gases, with the option of imposing polarity switching in the axial dc electric field. The plasma chamber is comprised of three 30-mm-diameter glass tubes connected in a π-shaped configuration. A 200-mm working area is located in the central part of the main tube, visualized by two particle observation cameras and a plasma glow observation camera. An illumination laser and manipulation laser are positioned at either end of the main tube, and three dust shakers for dispensing micrometer-sized grains are located on each of the two side tubes. A schematic of the PK-4 experiment is shown in Fig. 1, and further details may be found in Ref. [13]–[15].

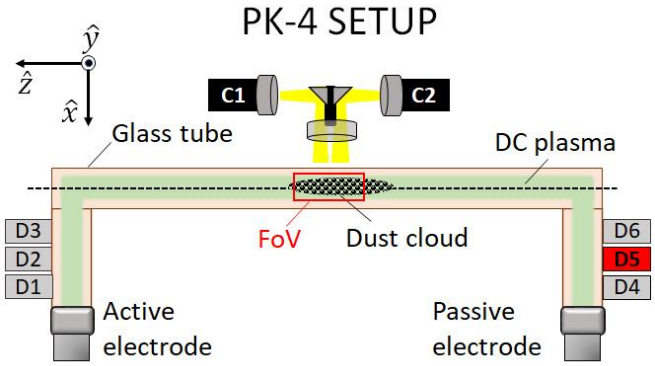

Fig. 1 Schematic of the PK-4 experiment indicating the location of the particle observation cameras (C1 and C2), dust shakers (D1-D6), the field of view in the working area (FoV), and relative orientation of the three glass tubes.

Dust grains immersed in the PK-4 plasma are subject to acceleration by the axial electric field. In order to trap dust grains in the central field of view for video observation, the polarity of the dc electric field is alternated uniformly at a sufficiently high frequency that the dust grains are unable to respond to the changing field direction, typically 500 Hz. However, the less massive ions can respond to changing conditions at timescales on the order of microseconds, and the changing electric field direction causes the ions to flow past the relatively stationary dust grains during both phases of the polarity switching. Positively charged ions flowing past a negatively charged dust grain will be deflected, forming a region of enhanced ion density downstream from the dust grain known as an ion wake, illustrated in Fig. 2. In addition to trapping the dust grains within the field of view, it was also observed that applying uniform polarity switching of the axial electric field caused the dust grains to align in long filamentary structures [16], like those shown in Fig. 3 (reproduced from Figure 9 in Ref. [17]). The accumulation of excess positive charge in the ion wake can

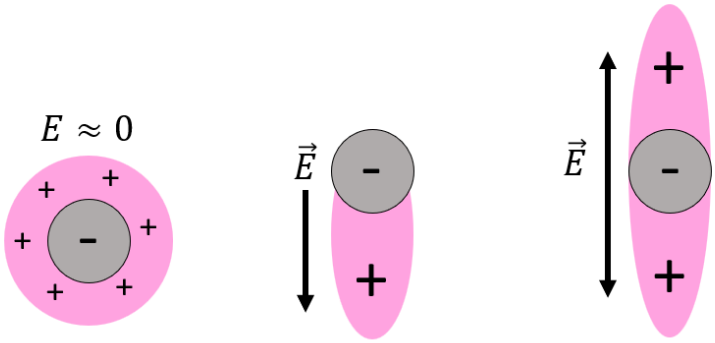

Fig. 2 Illustration of ion distribution (pink) around a negatively charged dust grain (gray) in the case of no applied electric field (left), a dc electric field with no polarity switching (center), and an electric field with uniform polarity switching (right).

influence other charged dust grains and has been suggested as a mechanism responsible for the organization of dust grains into experimentally observed structures [18]–[21].

III. DRIAD Molecular Dynamics Simulation

The interaction between ions and dust grains in a complex plasma leads to dynamically evolving ion wakes, where the fluctuating dust charge influences the charge and spatial extent of the ion wake while the ion wake mediates interactions between dust grains. However, the substantial numbers of ions present in a dusty plasma experiment, typically in excess of 10^{10} in the working area of the PK-4 alone, renders an analytic determination of the system's evolution practically impossible. As early as the 1950s, molecular dynamics (MD) simulations were being developed to address the problem of precisely calculating the individual motions of a large number of mutually interacting particles (the so-called "N-body" problem) [22]. The time to execute MD simulations has since been further accelerated by implementing parallel processing techniques with modern graphic processing units (GPUs), which are capable of performing thousands of calculations simultaneously [23].

The Dynamic Response of Ions and Dust (DRIAD) is an N-body molecular dynamics (MD) simulation designed to model the dusty plasma environment in typical ground-based laboratory experiments as well as the PK-4. DRIAD is capable of modeling the motions of individual dust grains and ions on their own timescales, as well as the dynamic charging of dust grains [24]. In order to focus on the relevant time and spatial scales for dust and ion dynamics, the electrons are treated as a fluid governed by a Boltzmann distribution and not directly modeled by the simulation. As ions and dust grains move throughout the simulation region, the forces acting on each particle are calculated in response to the spatially and temporally evolving ion number density in the ion wakefield and evolving dust grain charge. At the same time, the dust grain charge is dynamically updated based on the sum of the ion and electron currents to the dust grain. The ion current is directly modeled by tracking the number of ions that cross the collection radius of the dust grain, while the electron current is calculated using orbit motion limited (OML) theory [17], [24], [25].

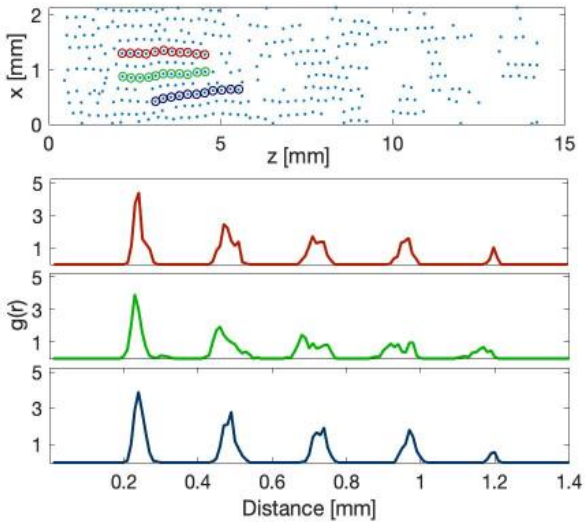

Fig. 3 Visualization of experimental results from campaign 7 of the PK-4 experiment illustrating the location of three selected dust chains (top panel) and the corresponding pair correlation functions for the highlighted chains (lower three panels). (Figure reproduced from Figure 9 in Ref. [17].)

The motions of ions and dust grains occur on timescales that differ by many orders of magnitude ($\Delta t_d \approx 0.1$ ms, and $\Delta t_i \approx 0.01$ μs), which can make it difficult to model both species with a single simulation.

The method used by DRIAD follows a two-step process: First, ions move and reach an equilibrium distribution over 100-1000 Δt_i in the presence of stationary dust grains; second, the ions' positions are fixed while the dust grains move for one Δt_d in the new ion distribution. The iterative process of moving only the ions followed by moving only the dust grains continues until the dust and ions have reached equilibrium, with the number of dust time steps required to reach a static or dynamic equilibrium varying based on the specific conditions being simulated.

DRIAD is implemented using an asymmetric molecular dynamics scheme following the method described by Piel [28], where the force on dust grains from ions is calculated from a shielded Coulomb interaction, and the force on ions from dust grains is calculated using a bare Coulomb potential. This method is intended to account for the continuum of electron shielding that ranges from the region far from the dust grain where $n_e \approx n_i$ to the region of electron depletion near the dust grains and has been found to reasonably reproduce ion-dust interparticle forces calculated from PIC simulations [29]. Further details about the DRIAD simulation and capabilities can be found in Ref. [24].

The motion of ions with mass m_i and charge q_i is governed by the equation of motion

$$m_i \ddot{\vec{r}}_i = \vec{F}_{ij} + \vec{F}_{iD} + \vec{F}_E(z) + \vec{F}_{\text{bound}}(r,z) + \vec{F}_{in} \tag{1}$$

Here, the force between ions i and j separated by a distance r_{ij} is calculated using an expression derived from the Yukawa potential, with the electrons providing the shielding of characteristic length λ_{De}

$$\vec{F}_{ij} = \sum_{i \neq j}^{N_i} \frac{q_i q_j}{4\pi\varepsilon_0 r_{ij}^3}\left(1 + \frac{r_{ij}}{\lambda_{De}}\right)\exp\left[-\frac{r_{ij}}{\lambda_{De}}\right]\vec{r}_{ij}\,. \tag{2}$$

The force acting on the i^{th} ion from the dust grains with charge Q_d, $\vec{F}_{iD}$, is calculated using an expression derived from the Coulomb potential of the form, as the Boltzmann-distribution electrons are depleted in the region near the negatively charge dust

$$\vec{F}_{iD} = \sum_{d}^{N_d} \frac{q_i Q_d}{4\pi\varepsilon_0 r_{id}^3}\vec{r}_{id}\,. \tag{3}$$

The ions experience a force from the axial electric field, $\vec{F}_E(z)$, which may include polarity switching according to the user input. Since the simulation represents only a small region in the larger plasma discharge, it is also necessary to account for the plasma surrounding the simulated region. Interaction with the background plasma is included in DRIAD through a bounding force, $\vec{F}_{\text{bound}}(r,z)$, which is calculated from the potential gradient within the simulation region due to a uniform distribution of ions outside the simulation region. The force from ion-neutral collisions, $\vec{F}_{in}$, is incorporated using the null-collision method [26], which improves computational efficiency by reducing the number of times the simulation "checks" for a collision between the ions and neutral atoms. Computational efficiency is further improved by modeling superions with the same charge-to-mass ratio as an individual ion (and therefore obeying the same equation of motion) but which represent a number of individual ions. One superion typically represents approximately 200 individual ions, with the exact number of ions per superion set by the user.

Dust grains with mass m_d in the DRIAD simulation move in accordance with the equation of motion

$$m_d \ddot{\vec{r}}_d = \vec{F}_{di} + \vec{F}_{dD} + \vec{F}_E(z) + \vec{F}_{\text{drag}} + \vec{F}_B + \vec{F}_C. \tag{4}$$

The force acting on dust from the ions in the simulation, $\vec{F}_{di}$, is calculated from a Yukawa potential similar to Eq. (2), which is averaged over the ion timesteps occurring between each dust timestep. The shielding of dust grains by ions is accounted for by the force $\vec{F}_{di}$ in DRIAD, so the force between dust grains, $\vec{F}_{dD}$, uses a Coulomb interaction similar to Eq. (3). The charged dust grains are subject to the same axial electric field force as the ions, $\vec{F}_E(z)$, as well as a neutral gas drag force, $\vec{F}_{\text{drag}} = \beta\dot{\vec{r}}$, which depends on the temperature and pressure of the neutral gas, where the coefficient is

$$\beta = 1.44\left(\frac{4a^2P_g}{3m_d}\right)\sqrt{\frac{8\pi m_i}{k_B T_g}} \tag{5}$$

where m_i is the mass of an ion and T_g is the temperature of the neutral gas at pressure P_g. The dust grains are subject to a random kick to simulate being immersed in a thermal bath, $\vec{F}_B = \zeta \mathrm{R}(t)$, where the coefficient $\zeta = \sqrt{2\beta k_B T_g/(m_d \Delta t_d)}$ determines the maximum force imparted by an individual kick, and $\mathrm{R}(t)$ is a random number selected using the Box-Muller transform method [27].

$$\mathrm{R}(t) = \sqrt{-2\ln U_1}\cdot\cos(2\pi U_2) \tag{6}$$

where U_1 and U_2 are random numbers between 0 and 1 generated by the C++ rand() function. The confining force, $\vec{F}_C$, accounts for the dust confinement due to the particular experimental conditions being simulated, which can include confinement imposed by stationary objects placed in the plasma discharge or neighboring dust particles outside the simulation region.

IV. Simulating the PK-4 Discharge

The positive column of the plasma generated in the PK-4 experiment appears to be uniform and homogeneous at the timescales observed by the onboard imaging equipment. However, PIC simulations of the plasma conditions present in the PK-4 have revealed the presence of fast-moving inhomogeneous features, or "ionization waves" [30]. High-speed video data obtained using a ground-based analogue of the flight version of the PK-4, the PK-4 BU [31], confirmed the presence of ionization waves, as seen in Fig. 4 (reproduced from Figure 4 in [30]). The ionization waves were seen to move through the positive column with phase velocities from 500 – 1,200 m/s and resulted in variations by as much as ten times background values in the electric field strength and particle density values. A representative time series of the electric field strength, electron and ion number density, and electron and ion temperature is provided in Fig. 5, with all values shown normalized to the maximum value attained during the visualized time interval.

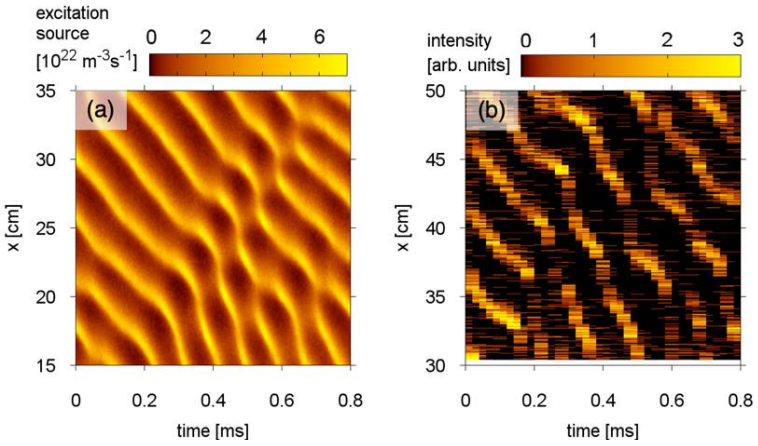

Fig. 4 PIC simulation results (a) and experimental data (b) illustrating the fast-moving ionization waves present in PK-4 conditions. (reproduced from Figure 4 of Ref. [30].)

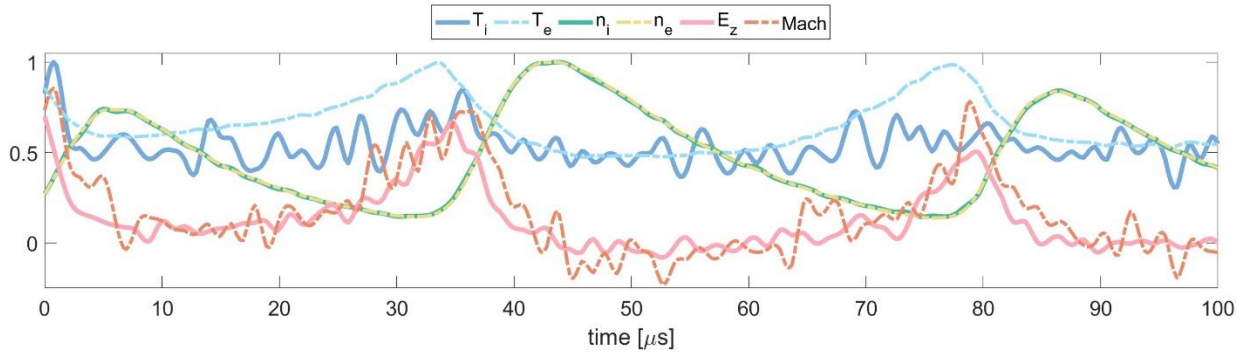

Fig. 5 Results from the PIC simulation of PK-4 conditions at 60 Pa showing the variation in ion and electron temperature (T_i and T_e), ion and electron density (n_i and n_e), axial electric field (E_z), and ion sound speed Mach (Mach) as ionization waves pass through the plasma. All quantities are normalized to their maximum value.

A. Simulating Dust Chains in the PK-4

Video data obtained from the PK-4 experiment indicated the presence of extended filamentary dust structures, called "dust chains." The dust chains form along the axis parallel to the dc electric field during polarity switching, a phenomenon that is theorized to be related to the interaction of negatively charged dust grains with the positively charged ion wakes of other dust grains. A representative frame from video data collected in the PK-4 experiment is shown in the top panel of Fig. 3, with chains selected for analysis highlighted in red, green, and blue circles. The bottom three panels in Fig. 3 show the pair correlation for the three chains highlighted in the top panel, with the line colors indicating the chain used for analysis (reproduced from Figure 9 in [17]).

Dust grains immersed in the PK-4 experiment can respond to changes in the plasma environment on a timescale of a few milliseconds, so a naïve assumption would be that the plasma can be reasonably modeled using the time average of the local plasma density and temperature. However, this assumption was shown to be inconsistent with simulation results that investigated the ionization wave characteristics obtained from the PIC simulation [17], [25].

DRIAD was used to simulate the plasma conditions present in the PK-4 and investigate the charging of dust and subsequent formation of single particle chains. Twenty dust grains were initially placed in a region approximately 0.45 mm in diameter near the center of an 0.84 mm × 8.05 mm cylindrical simulation region. The dust grains were then allowed to move freely in the simulation region and charge in response to the evolution of ion wakes. At the same time, the locations and density of the ions in the ion wakefields responded to the positions and charge of the dust grains.

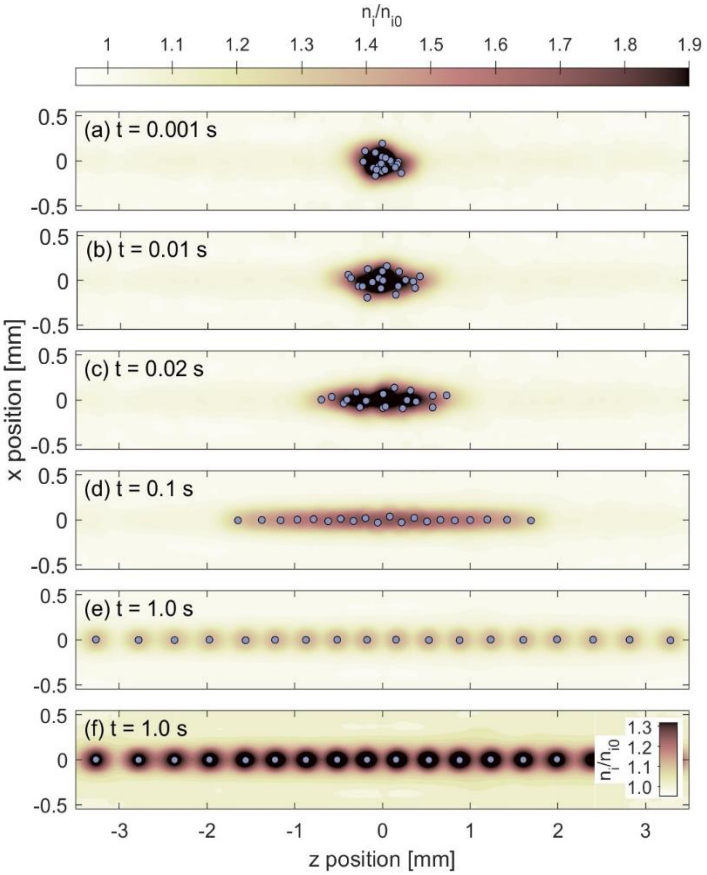

Fig. 6 Time evolution of dust positions (gray circles) and associated ion density. The shading indicates the ion density normalized to the background ion density (4.432×10^{14} $\mathbf{m^{-3}}$). The bottom panel (f) shows the same time as (e) with a smaller range of contour colors to highlight details in the ion wake surrounding the equilibrium dust chain.

The normalized ion density at the simulation times 0.001 s, 0.01 s, 0.02 s, 0.1 s, and 1.0 s are illustrated in Fig. 6a-e, where gray circles indicate dust grains and the ion density normalized to the background ion density (4.43×10^{14} m^{-3}) is indicated by the shading. The simulation at 1.0 seconds (shown in Fig. 6e) is reproduced in Fig. 6f with a smaller contour range to highlight the overlapping ion wakes found between dust grains along the dust chain.

The pair correlation function, $g(r)$, is a useful tool for analyzing the order of the dust grains within the chain, and is defined using the equation

$$g(r) = \frac{1}{\rho}\left\langle \sum_{i \neq j} \delta\left(r - r_{ij}\right) \right\rangle \tag{7}$$

where ρ represents the number of particles per volume, and r_{ij} represents the distance between particles i and j. The pair correlation function represents the probability of finding a neighbor particle at a distance r and provides

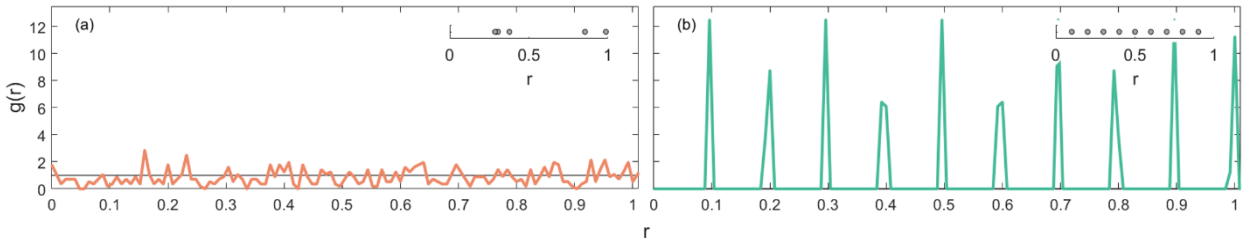

Fig. 7 Example g(r) plots illustrating particles distributed (a) randomly and (b) at even intervals, with positions of the particles in the range $0 \leq r \leq 1$ shown by the gray circles in the inset plot in each panel.

information about the order of the collection of particles. A completely random distribution of particles has a pair correlation trending to one (indicating the particles are in a gaseous state with uncorrelated positions), while a regular distribution of particles appears as a series of sharp peaks (illustrated in Fig 7a and b, respectively).

The pair correlation functions calculated for simulated dust chains using time-averaged plasma conditions reveal that time-averaged conditions did not reproduce the degree of order seen in experimental conditions, as shown by the green line in Fig. 8. However, using the plasma conditions present during the peak axial electric field in the ionization waves produces dust chains with stronger and more well-defined peaks in $g(r)$, indicated by the yellow line in Fig. 8. This suggests that although the dust grains respond on the millisecond timescale, the variations occurring on the microsecond timescale have a significant influence on the ordering of the dust structures. The finite charging and discharging time as ionization waves pass was shown to produce a lower average charge than the averaged plasma conditions, which leads to a weaker repulsive force between grains and smaller interparticle spacing that more closely matches the results from the PK-4 experiment [17].

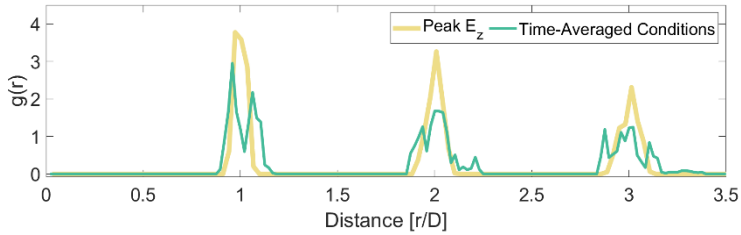

Fig. 8 Comparison between $g(r)$ calculated for the dust chain formed with time-averaged plasma conditions (green) and conditions present during the peaks in the axial electric field (yellow). The distance, r, is normalized to average interparticle spacing, D.

B. Simulating Large Dust Clouds

In addition to the observed filamentary dust chains that form along the discharge tube axis, the dust grains in the PK-4 experiment have been observed to form large dust clouds measuring several millimeters radially and extending for centimeters along the tube axis. These large dust clouds can display interesting collective behavior, including the formation of boundary layers, shock waves, and dust particle lanes.

The DRIAD simulation was used to model the dynamics and charging of extended dust clouds under the evolving plasma conditions found in ionization waves, which provided three-dimensional dust grain positions as well as information about the local ion density variation at the sub-millisecond timescale. These details have relevance for studying the development of laning structures observed not only in the large dust clouds in the PK-4 experiment, but also in systems as wide-ranging as pedestrian flows, army ants, and self-driven microswimmers in colloidal suspensions [32]–[34]. The simulation modeled 1000 dust grains in a cylindrical region with a radius of 0.90 mm and length of 5.42 mm, with boundary conditions imposed to confine dust grains to the central six Debye lengths (≈ 2.7 mm) in the axial direction. The dust grain positions and charges were allowed to evolve to equilibrium, and analysis of the final structure revealed the formation of dust particle lanes as well as nested cylindrical shells. A view of the final dust positions from one axial end is provided in the left panel of Fig. 9, illustrating the cylindrical shells formed in the simulated dust cloud. The side view of a 0.14-mm-wide slice along the z-axis is provided in the right panel of Fig. 9.

The dust grains contained in each of the nested cylinders also possess hexagonal ordering that can be seen when the cylinders are "unwrapped" by plotting the dust positions around the circumference of the nested cylinder ($s = r\theta$)

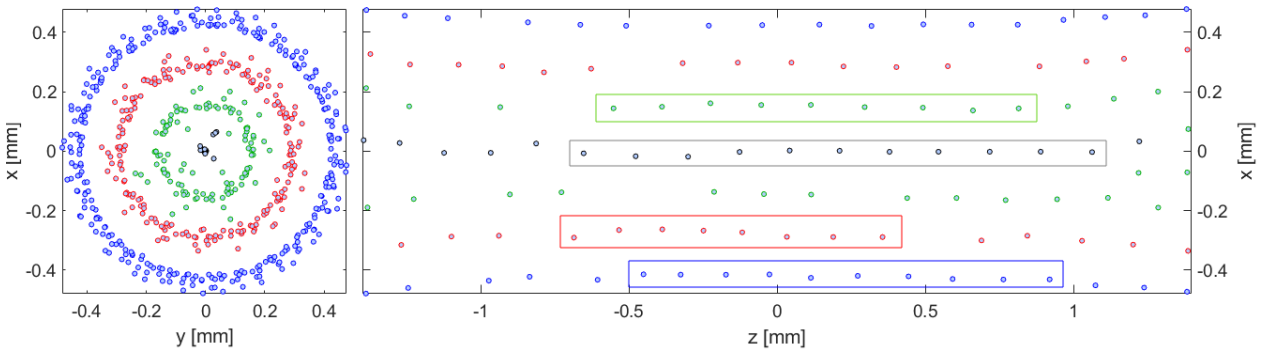

Fig. 9 Simulation of a 1000 dust grain cloud in the PK-4, viewed from the axial end, showing dust arranged into nested cylinders (left) and slice through the mid-plane, showing the arrangement of grains in filamentary structures (right). Individual dust positions are indicated by the light gray circles with outline colors indicating the dust grains belonging to the outermost cylinder (blue), middle cylinder (red), and innermost cylinder (green). Circle size does not indicate the size of the dust grains. Representative chain-like structures found in the mid-plane are highlighted by the rectangles in the right panel.

vs. the axial position (z), as shown in Fig. 10. The unwrapped dust positions show the dust forming 2D hexagonal lattices, indicating order in the directions parallel and perpendicular to the electric field direction.

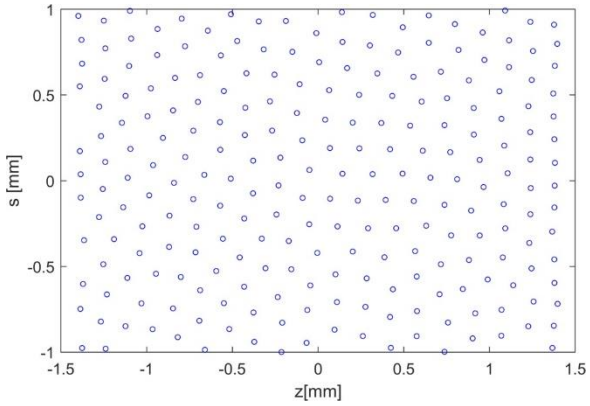

Fig. 10 Unwrapped dust grain positions for outermost cylinder in Fig. 9 plotted as circumferential position (s) vs. axial position (z).

The order observed in the large dust clouds can be characterized using a pair correlation function that takes into account the three-dimensional nature of the dust cloud. Using the pair correlation function in spherical coordinates, as introduced in Ref. [35], with the form

$$G(r,\theta,\phi) = \frac{1}{n_d N} \sum_{\substack{i,j=1 \\ i \neq j}}^{N} \frac{\delta(r_{ij} - r)\delta(\theta_{ij} - \theta)\delta(\phi_{ij} - \phi)}{4\pi r^2 \cos(\theta)} \tag{8}$$

provides two dimensional particle distributions by integrating over the azimuthal angle ϕ:

$$G_{\phi}(r,\theta) = \int_0^{2\pi} G(r,\theta,\phi) d\phi \tag{9}$$

or the polar angle θ:

$$G_\theta(r,\phi) = \int_{-\frac{\pi}{2}}^{\frac{\pi}{2}} G(r,\theta,\phi)\cos(\theta)\,d\theta \tag{10}$$

where n_d is the dust number density and N represents the number of dust grains.

Analysis of the dust grain positions in the simulation of the large dust cloud yields the two dimensional distributions shown in Fig. 11, where bright regions correspond to larger calculated pair correlation values. The bright vertical bands in the left panel of Fig. 11 indicate regular interparticle spacing of ~155 μm between dust grains within a chain. The narrow localized peaks in the first band indicate more uniform spacing between nearest neighbors, while the wide or diffuse vertical bands indicate less order in the second- or third-nearest neighbors. Peaks appearing in the $G_\theta(r,\phi)$ distribution along the ϕ axis (within a vertical band) indicate the order between neighboring dust chains (perpendicular to the axial electric field direction), with localized peaks indicating a high degree of alignment between dust chains while a diffuse band along the ϕ axis indicates decreased interchain alignment.

Dust grains in filaments aligned with the axial electric field (coincident with the symmetry axis in the simulation cylinder) will generate peaks in the $G_\phi(r,\theta)$ distribution at polar angles $\theta = \pm\pi/2$ at a distance r corresponding to integer multiples of the intrachain dust particle spacing (Fig. 11b). Polar angles $\theta < |\pi/2|$ in the $G_\phi(r,\theta)$ distribution correspond to the correlation between chains, with well-defined peaks indicating alignment of dust grains perpendicular to the cylinder axis while the appearance of smooth arches indicates more random axial positioning of dust grains in neighboring chains.

Comparing the distribution analysis obtained in Fig. 11 with the dust cloud shown in Fig. 9 and 10 provides further insight about the cloud structure. While the dust grains are grouped into large, nested cylinders, the position of a dust grain with respect to grains in an adjacent cylinder is less ordered (seen as a smooth band for the range of ϕ values in the left plot of Fig. 11). Additionally, the hexagonal lattice that appears when the nested cylinders are "unwrapped" produces increased alignment of dust grains in neighboring chains (seen as localized bright peaks at $\theta < |\pi/2|$ in the right plot of Fig. 11).

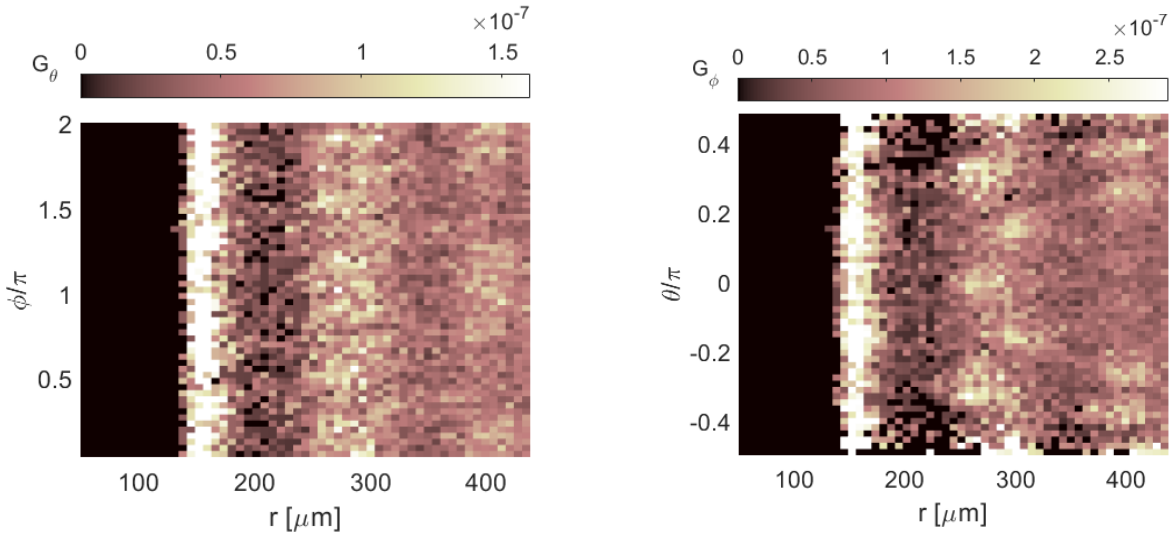

Fig. 11 Three-dimensional pair correlation functions a) $G_\theta(r,\phi)$ and b) $G_\phi(r,\theta)$ calculated for a cloud consisting of 1700 dust particles.

V. Conclusion

Dust grains in the microgravity environment of the PK-4 experiment can levitate in the plasma bulk where the smaller ion-dust and dust-dust forces dominate particle interactions. Numerical models of the PK-4 experiment provide insight into the influence that dynamically evolving plasma conditions within ionization waves have on the ion wakes and subsequent formation of dust microstructures. Simulation results reveal that the observed structure imposed on the dust cloud are the results of asymmetric particle interactions mediated by ion wakes. The formation

of the wakes is related to the presence of strong electric fields present in ionization waves. The ion flow driven by the strong electric fields also alters the equilibrium dust charge. Simulations that incorporate temporal and spatial variations in the background plasma parameters are currently in progress and are expected to provide further details about the plasma-mediated dynamic interactions between charged dust grains.

Acknowledgments

Support for this work from NSF grant numbers 1903450 and 1740203, NASA grant number 1571701, and the U.S. Department of Energy, Office of Science, Office of Fusion Energy Sciences under award number DE-SC-0021334. All authors gratefully acknowledge the joint ESA - Roscosmos "Experiment Plasmakristall-4" onboard the International Space Station. The microgravity research is funded by the space administration of the Deutsches Zentrum für Luft- und Raumfahrt eV with funds from the federal ministry for economy and technology according to a resolution of the Deutscher Bundestag under Grants No. 50WM1441 and No. 50WM2044.

References

[1] J. M. Long and J. Ou, "Dust particle surface potential in fusion plasma with supra-thermal electrons," *Phys. Plasmas*, vol. 29, no. 9, p. 093701, Sep. 2022, doi: 10.1063/5.0091856.

[2] G. S. Selwyn, J. Singh, and R. S. Bennett, "In Situ laser diagnostic studies of plasma-generated particulate contamination," *J. Vac. Sci. Technol. Vac. Surf. Films*, vol. 7, no. 4, pp. 2758–2765, Jul. 1989, doi: 10.1116/1.576175.

[3] J. H. Chu and L. I, "Direct observation of Coulomb crystals and liquids in strongly coupled rf dusty plasmas," *Phys. Rev. Lett.*, vol. 72, no. 25, pp. 4009–4012, Jun. 1994, doi: 10.1103/PhysRevLett.72.4009.

[4] J. Carstensen, F. Greiner, D. Block, J. Schablinski, W. J. Miloch, and A. Piel, "Charging and coupling of a vertically aligned particle pair in the plasma sheath," *Phys. Plasmas*, vol. 19, no. 3, p. 033702, Mar. 2012, doi: 10.1063/1.3689854.

[5] J. Goree, "Charging of particles in a plasma," *Plasma Sources Sci. Technol.*, vol. 3, no. 3, pp. 400–406, Aug. 1994, doi: 10.1088/0963-0252/3/3/025.

[6] M. Y. Pustylnik, A. A. Pikalev, A. V. Zobnin, I. L. Semenov, H. M. Thomas, and O. F. Petrov, "Physical aspects of dust–plasma interactions," *Contrib. Plasma Phys.*, vol. 61, no. 10, p. e202100126, 2021, doi: 10.1002/ctpp.202100126.

[7] H. Thomas, G. E. Morfill, V. Demmel, J. Goree, B. Feuerbacher, and D. Möhlmann, "Plasma Crystal: Coulomb Crystallization in a Dusty Plasma," *Phys. Rev. Lett.*, vol. 73, no. 5, pp. 652–655, Aug. 1994, doi: 10.1103/PhysRevLett.73.652.

[8] O. Arp, D. Block, A. Piel, and A. Melzer, "Dust Coulomb Balls: Three-Dimensional Plasma Crystals," *Phys. Rev. Lett.*, vol. 93, no. 16, p. 165004, Oct. 2004, doi: 10.1103/PhysRevLett.93.165004.

[9] P. Hartmann *et al.*, "Crystallization Dynamics of a Single Layer Complex Plasma," *Phys. Rev. Lett.*, vol. 105, no. 11, p. 115004, Sep. 2010, doi: 10.1103/PhysRevLett.105.115004.

[10] P. Hartmann, A. Zs. Kovács, A. M. Douglass, J. C. Reyes, L. S. Matthews, and T. W. Hyde, "Slow Plastic Creep of 2D Dusty Plasma Solids," *Phys. Rev. Lett.*, vol. 113, no. 2, p. 025002, Jul. 2014, doi: 10.1103/PhysRevLett.113.025002.

[11] M. Bonitz, C. Henning, and D. Block, "Complex plasmas: a laboratory for strong correlations," *Rep. Prog. Phys.*, vol. 73, no. 6, p. 066501, Jun. 2010, doi: 10.1088/0034-4885/73/6/066501.

[12] G. E. Morfill and A. V. Ivlev, "Complex plasmas: An interdisciplinary research field," *Rev. Mod. Phys.*, vol. 81, no. 4, pp. 1353–1404, Oct. 2009, doi: 10.1103/RevModPhys.81.1353.

[13] V. Fortov *et al.*, "The project 'Plasmakristall-4' (PK-4)—a new stage in investigations of dusty plasmas under microgravity conditions: first results and future plans," *Plasma Phys. Control. Fusion*, vol. 47, no. 12B, pp. B537–B549, Dec. 2005, doi: 10.1088/0741-3335/47/12B/S39.

[14] H. M. Thomas *et al.*, "Complex plasma research on the International Space Station," *Plasma Phys. Control. Fusion*, vol. 61, no. 1, p. 014004, Jan. 2019, doi: 10.1088/1361-6587/aae468.

[15] M. Y. Pustylnik *et al.*, "Plasmakristall-4: New complex (dusty) plasma laboratory on board the International Space Station," *Rev. Sci. Instrum.*, vol. 87, no. 9, p. 093505, 2016, doi: 10.1063/1.4962696.

[16] A. V. Ivlev, M. H. Thoma, C. Räth, G. Joyce, and G. E. Morfill, "Complex Plasmas in External Fields: The Role of Non-Hamiltonian Interactions," *Phys. Rev. Lett.*, vol. 106, no. 15, p. 155001, Apr. 2011, doi: 10.1103/PhysRevLett.106.155001.

[17] K. Vermillion *et al.*, "Influence of temporal variations in plasma conditions on the electric potential near self-organized dust chains," *Phys. Plasmas*, vol. 29, no. 2, p. 023701, Feb. 2022, doi: 10.1063/5.0075261.

[18] A. Melzer, V. A. Schweigert, I. V. Schweigert, A. Homann, S. Peters, and A. Piel, "Structure and stability of the plasma crystal," *Phys. Rev. E*, vol. 54, no. 1, pp. R46–R49, Jul. 1996, doi: 10.1103/PhysRevE.54.R46.

[19] A. Melzer, V. A. Schweigert, and A. Piel, "Transition from Attractive to Repulsive Forces between Dust Molecules in a Plasma Sheath," *Phys. Rev. Lett.*, vol. 83, no. 16, pp. 3194–3197, Oct. 1999, doi: 10.1103/PhysRevLett.83.3194.

[20] A. V. Ivlev *et al.*, "First Observation of Electrorheological Plasmas," *Phys. Rev. Lett.*, vol. 100, no. 9, p. 095003, Mar. 2008, doi: 10.1103/PhysRevLett.100.095003.

[21] A. V. Ivlev *et al.*, "Electrorheological Complex Plasmas," *IEEE Trans. Plasma Sci.*, vol. 38, no. 4, pp. 733–740, Apr. 2010, doi: 10.1109/TPS.2009.2037716.

[22] B. J. Alder and T. E. Wainwright, "Studies in Molecular Dynamics. I. General Method," *J. Chem. Phys.*, vol. 31, no. 2, pp. 459–466, Aug. 1959, doi: 10.1063/1.1730376.
[23] J. Nickolls and W. J. Dally, "The GPU Computing Era," *IEEE Micro*, vol. 30, no. 2, pp. 56–69, Mar. 2010, doi: 10.1109/MM.2010.41.
[24] L. S. Matthews, D. L. Sanford, E. G. Kostadinova, K. S. Ashrafi, E. Guay, and T. W. Hyde, "Dust charging in dynamic ion wakes," *Phys. Plasmas*, vol. 27, no. 2, p. 023703, Feb. 2020, doi: 10.1063/1.5124246.
[25] L. S. Matthews *et al.*, "Effect of ionization waves on dust chain formation in a DC discharge," *J. Plasma Phys.*, vol. 87, no. 6, p. 905870618, Dec. 2021, doi: 10.1017/S0022377821001215.
[26] Z. Donko, "Particle simulation methods," *Plasma Sources Sci Technol*, p. 16, 2011.
[27] G. E. P. Box and M. E. Muller, "A Note on the Generation of Random Normal Deviates," *Ann. Math. Stat.*, vol. 29, no. 2, pp. 610–611, 1958.
[28] A. Piel, "Molecular dynamics simulation of ion flows around microparticles," *Phys. Plasmas*, vol. 24, no. 3, p. 033712, Mar. 2017, doi: 10.1063/1.4978791.
[29] I. H. Hutchinson, "Intergrain forces in low-Mach-number plasma wakes," *Phys. Rev. E*, vol. 85, no. 6, p. 066409, Jun. 2012, doi: 10.1103/PhysRevE.85.066409.
[30] P. Hartmann *et al.*, "Ionization waves in the PK-4 direct current neon discharge," *Plasma Sources Sci Technol*, p. 16, 2020.
[31] J. Schmidt and T. W. Hyde, "Discharge parameters of PlasmaKristall-4BU: A modifiable dusty plasma experiment," *Rev. Sci. Instrum.*, vol. 91, no. 8, p. 083506, Aug. 2020, doi: 10.1063/5.0005325.
[32] I. D. Couzin and N. R. Franks, "Self-organized lane formation and optimized traffic flow in army ants," *Proc. R. Soc. Lond. B Biol. Sci.*, vol. 270, no. 1511, pp. 139–146, Jan. 2003, doi: 10.1098/rspb.2002.2210.
[33] D. Zhang, H. Zhu, S. Hostikka, and S. Qiu, "Pedestrian dynamics in a heterogeneous bidirectional flow: Overtaking behaviour and lane formation," *Phys. Stat. Mech. Its Appl.*, vol. 525, pp. 72–84, Jul. 2019, doi: 10.1016/j.physa.2019.03.032.
[34] F. Kogler and S. H. L. Klapp, "Lane formation in a system of dipolar microswimmers," *EPL Europhys. Lett.*, vol. 110, no. 1, p. 10004, Apr. 2015, doi: 10.1209/0295-5075/110/10004.
[35] M. Y. Pustylnik *et al.*, "Three-dimensional structure of a string-fluid complex plasma," *Phys. Rev. Res.*, vol. 2, no. 3, p. 033314, Aug. 2020, doi: 10.1103/PhysRevResearch.2.033314.